

## ARTICLES

## Self-Assembly of Gold Nanorods

B. Nikoobakht,<sup>†</sup> Z. L. Wang,<sup>‡</sup> and M. A. El-Sayed<sup>\*,†</sup>*Laser Dynamics Laboratory, School of Chemistry and Biochemistry, and School of Materials Science and Engineering, Georgia Institute of Technology, Atlanta, Georgia 30332-0400**Received: April 3, 2000; In Final Form: June 27, 2000*

Self-assembly of gold nanorods (NRs) with aspect ratio of  $\sim 4.6$  (12 nm in diameter and 50–60 nm in length) has been studied using transmission electron microscopy (TEM). Under appropriate conditions such as nanoparticle concentration, solvent evaporation, narrow size distribution, ionic strength, and surfactant concentration of the parent solution, gold nanorods assemble into one-, two-, and three-dimensional structures. Some of the three-dimensional assemblies extend to superlattices of NRs. The translation and orientation symmetries of the self-assembled structures are determined. The factors affecting the formation of the ordered self-assembly are discussed.

## Introduction

Nanoparticles are attracting a great deal of attention due to their potential applications in optics, electronics, and catalysis.<sup>1</sup> Two important directions of research in this field are the synthesis and self-assembly of nanoparticles. In the synthetic direction, dozens of methods have been developed to synthesize metallic and semiconductor nanoparticles of different shapes and sizes.<sup>2–4</sup> The design and preparation of organized and aligned particles have been another important active research direction.

In the synthesis of new materials based on an ordered assembly of nanocrystallites (quantum dots), two significant factors are important, namely the shape and size distributions of the nanoparticles.<sup>5</sup> Impressive accomplishments in the area of self-assembly of metallic silver and gold nanodots,<sup>6,7</sup> semiconductor CdSe<sup>8</sup> and Ag<sub>2</sub>S<sup>9</sup> quantum dots and spherical nanoparticles have been reported. A third important factor in the assembly of nanocrystals is the softness of the nanocrystals. The thickness and type of organic capping material can influence the type of packing of the particles in a superlattice (bcc, fcc, hcp, ...).<sup>10</sup> The self-assembled structure may possess interesting new collective physical properties that are different from those of the original bulk material.<sup>11–13</sup>

In spite of the large volume of research on the self-assembly of quantum dots, little attention has been devoted to the self-assembly of rod-shaped nanoparticles. One of the few examples is the self-assembly of prolate silver nanoparticles capped with thiol groups.<sup>14</sup> The particles have an aspect ratio of 1.4 and were prepared using two-phase solution and growth of nanoparticles in the organic phase.<sup>4a,b</sup> These particles produce two-dimensional assemblies with wirelike structure.

In the present work, we study the self-assembly of gold nanorods with length of 55 nm and width of 12 nm, i.e., an aspect ratio of  $\sim 4.6$ , capped by surfactant. We observe that

under certain conditions, these nanorods self-assemble into 1D, 2D, and 3D, leading to the formation of superlattices of NRs. TEM and electron diffraction were used to characterize the assemblies. Possible models are discussed in an attempt to explain the mechanism of the self-assembly of NRs in the observed structures.

## Synthesis of Gold Nanorods

Gold nanorods were prepared by an electrochemical method,<sup>15</sup> in which a gold electrode is used as the sacrificial anode and a platinum electrode as the cathode. The electrolyte consists of a mixture of hexadecyltrimethylammonium bromide (HTAB) as the cationic surfactant and tetraoctylammonium bromide as the cosurfactant; the mixture is dissolved in water. The latter surfactant induces the cylindrical shape of the gold nanoparticle and the ratio of the two surfactants determines the aspect ratio (the ratio of length to width) of the nanorod. The electrolysis is carried out under continuous ultrasonication and an applied current of 3–5 mA for about 45 min. TEM results show that the deposition of a portion of the as-prepared sample does not produce ordered self-assemblies but produces a coagulated structure of NRs. To facilitate self-assembly, further manipulation is required, as described below.

## Preparation of Self-Assembled Samples

One volume of the as-prepared sample is diluted with three volumes of doubly distilled water. After centrifugation at 14 000 rpm for 25 min at room temperature, the supernatant is decanted. The remaining solution is diluted with distilled water to an optical density of 1.5–1.7 in a 5 mm cell.<sup>16</sup> In this manner, one can adjust the NRs' concentration and reduce the amount of excess surfactant in the solution. The final step is 1:1 dilution of the above solution with 0.1 M NaCl solution, where NaCl acts as an electrolyte.

Several methods were used for depositing the sample on the TEM grid. Among them, two techniques were found to give a

<sup>†</sup> Laser Dynamics Laboratory, School of Chemistry and Biochemistry.

<sup>‡</sup> School of Materials Science and Engineering.

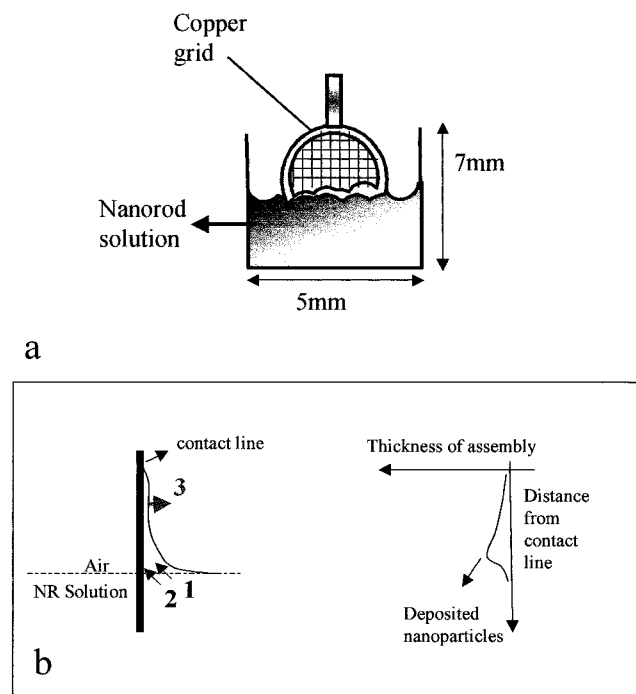


**Figure 1.** Scheme of the deposition method. The grid is inserted about one-quarter of the diameter of grid into the nanoparticle solution. The initial volume of the solution is  $\sim 100 \mu\text{L}$ . The thin film on the substrate rises up until the balance of hydrostatic pressure and the pressure inside the solution. Evaporation of water from the thin film causes influx of water (arrow 1) and particles from the bulk solution (arrow 2) to the thin film. The plot shows the trend in the thickness of the self-assembly.

large and ordered assembly. In the first method,  $4\text{--}5 \mu\text{L}$  of the nanoparticle solution was deposited on a carbon-coated TEM copper grid (as our substrate). The droplet dried in less than 1 h. In the second method, the grid was vertically inserted halfway into  $\sim 100 \mu\text{L}$  of the solution so that part of it was immersed into the solution (see Figure 1). The solvent evaporated, over 8 h. The TEM images showed reproducible self-assembly in most regions of the grid. It is noteworthy to mention that in terms of surface coverage and reproducibility, the latter method gives much better results than the former method. In other experiments, different positions of the copper grid were examined, such as total insertion of the grid into the solution or keeping the substrate horizontal under  $20 \mu\text{L}$  of the nanoparticle solution. After several trials, the results showed small assemblies of particles or large aggregates without ordered structure.

The structures of the self-assemblies were determined by transmission electron microscopy. Electron micrographs were acquired at 100 kV using JEOL100 or at 400 kV using JEOL 4000EX high-resolution TEM.

## Results

**Factors Affecting the Quality of Self-Assembly.** The results presented here are from the half-insertion method. Factors such as free surfactant concentration, ionic strength, particle concentration, particle shape, size distribution, and the position of the grid in the solution were varied in order to obtain organized assemblies.

Studies performed at various surfactant concentrations showed that high concentrations of surfactant may cause unwanted organic crystallites and/or a netlike organic structure between the particles. This inhibits the formation of ordered assemblies. On the other hand, reducing the free surfactant caused destruction of nanoparticles in the solution and on the substrate. Also the

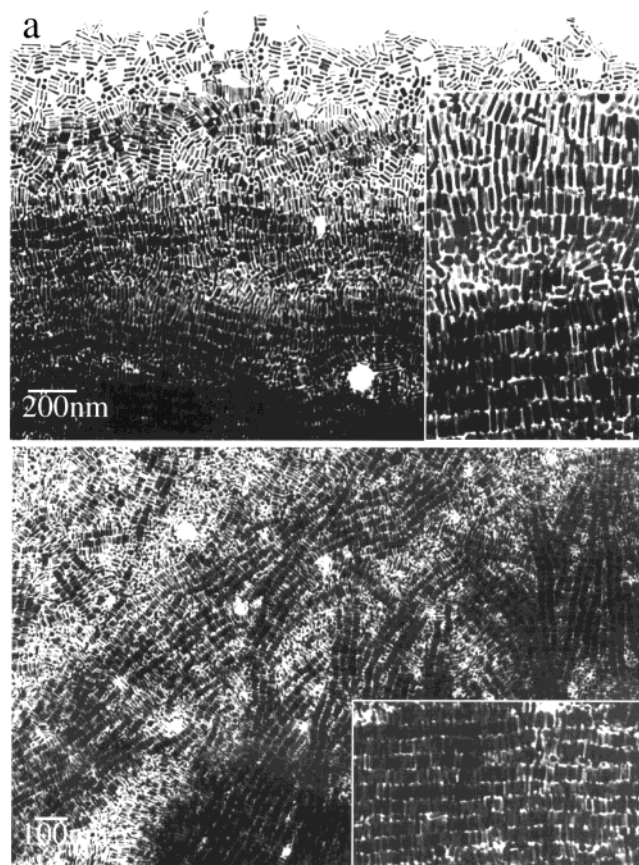


**Figure 2.** (a) Electron micrograph showing the border of the self-assemblies. The thickness increases from top to bottom. The inset shows a magnified part of an assembly; also it shows the presence of spherical particles can cause deviation in the shape of the self-assembly. (b) High tendency of forming long arrays visible in different areas of the substrate. The inset shows a superlattice of NRs.

TEM images showed that removal of the free surfactant increased the spacing between particles. The results of these experiments indicate that solutions with 0.001 M surfactant produced the most ordered structures.

To control the ionic strength of the solution, electrolytes such as NaCl, NaBr, NaI, and NaOH were used. TEM and UV-vis spectroscopy showed that a low concentration of NaCl is suitable for the purpose of self-assembly. Different concentrations of NaCl ranging from 0.025 to 0.5 M were used. At high ionic strength, such as 0.5 M, large assemblies were formed without any structure. In addition, at concentrations higher than 0.1 M, the nanoparticles on the grid were degraded in less than a few weeks. The best results were obtained at a concentration of 0.05 M NaCl.

Figure 2a shows a large area of the assembled NRs on the grid, which occurred at the water-air-substrate interface. Observation with an optical microscope and low magnification TEM images show that the self-assembly occurs in the vicinity of the region of the grid where the grid and solution intersect. If the grid is inserted completely into the same solution, as compared to partial insertion, much smaller areas of assembly occur. Moving along the grid, several regions can be distinguished. In the first micron region, close to the solution-substrate contact line, a monolayer of colonies of nanorod assemblies in a randomly oriented fashion is formed. The second region contains longer chains of NRs, which start forming two-dimensional assemblies. Further away from the initial contact line, in addition to developing the dimensionality of the assemblies on the grid plane, the thickness of the assemblies

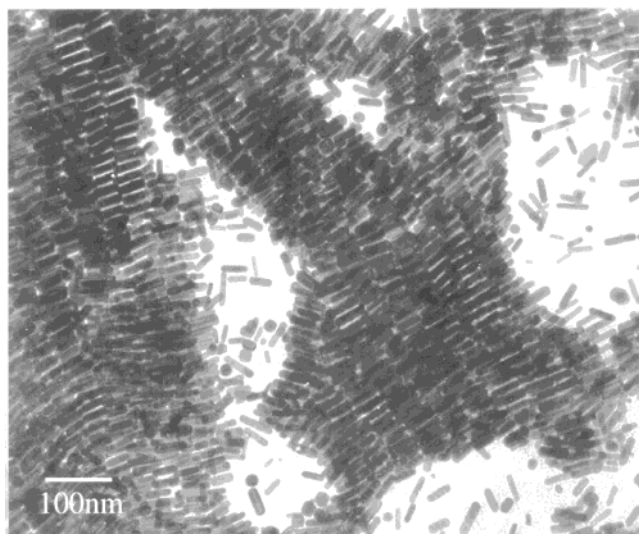


**Figure 3.** Assembly of NRs containing 3–4 layers of particles. The central part of the assembly is more ordered while the periphery of the assembly has a more disordered structure.

increases as well. An example of this pattern is seen in Figure 2a. Figure 2b shows the surface of the grid roughly about  $5 \mu\text{m}$  below the starting point of the self-assemblies. A continuous increase in size and thickness in this region produces very large superlattices of NRs. These superlattices are shown with darker color in the image. A typical three-dimensional superlattice of NRs is shown in the inset of Figure 2b.

Regions with low particle density between the assemblies appear on the substrate, as is illustrated at the bottom of Figure 2b. The TEM images show that after this region, the surface of the grid is covered with scattered nanoparticles and deposited surfactant from the solution. A decrease in the number, size, and thickness of self-assemblies could be an indication of a decrease in the particle supply of the solution or part of the solution near the substrate. The described pattern in self-assemblies was observed in several samples regardless of the rate of solvent evaporation and degree of organization of nanoparticles. This trend is shown in Figure 1.

It is important to point out that Figures 2a,b are obtained from the same grid and Figures 3 and 4 belong to a different TEM grid. These two sets of independent experiments were selected in order to show assemblies with different morphologies. The parent solutions for these two different grids are similar. An interesting characteristic of the assemblies in the second case is interconnected chains or arrays of NRs. The chains could be a single array of NRs or a more developed structure with several arrays in two dimensions (Figure 3). In some of these assemblies (Figure 4), along the array, the particles have different sizes. This variation in particle size is rarely seen in Figure 2a,b.

Inhomogeneous particle shape and size can be very important in determining the quality of the final form of the self-assembly. In the preparation of NRs, spherical particles are formed as a side product. These particles were mostly removed by centrifugation in order to improve the quality of the self-assemblies. Figure 2a and the inset show the effect of the presence of the spherical particles in some parts of the assembly. This can cause unequal spacing between arrays of NRs and consequently distort the 2- and 3- dimensional assemblies. In contrast, in regions with a low concentration of spherical particles, more regular forms of assemblies are observed; an example is seen in the inset of Figure 2b.

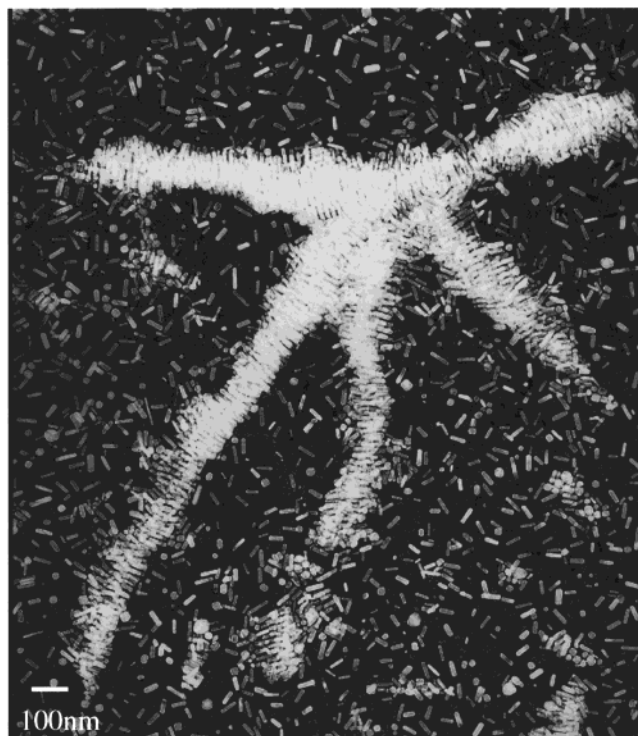


**Figure 4.** TEM image of the Rodman. Connected chains of rods grown in a radial fashion and wide size distribution of particles in a typical chain.

A variation in concentration of NRs produces assemblies of nanoparticles as well. At low concentrations, the TEM results show scattered nucleated sites of NRs, which have not been developed well. At high concentrations the assembly thickness is so large that it prevents the transmission of electrons.

**Orientation Order in Self-Assembly.** Self-assembly of nanoparticles exhibits not only translation symmetry but also orientational symmetry.<sup>17–19</sup> The orientation order occurs usually for nanoparticles with a well-defined shape, which reflects the degree of axial alignment of the nanorods. To model the type of packing of NRs, crystallographic description of a nanorod is necessary. The faceted shape of the gold nanorods was revealed previously by TEM.<sup>20</sup> The axial growth direction of a gold nanorod is  $[001]$ ; the circumference of the nanorod encloses eight crystallographic facets, i.e.,  $\{110\}$  and  $\{100\}$ . The presence of the flat facets is likely to introduce orientation order in the self-assembly. The present crystallographic study has been carried out on the sample, with assemblies shown in the TEM images shown in Figures 3 and 4.

Using a select area aperture, an electron diffraction pattern was recorded from an area of 500 nm in diameter. Figure 5a shows an electron diffraction pattern recorded from an area that contained  $\sim 200$  gold nanorods. The diffraction rings are from the diffraction of the crystal lattice rather than the superlattice of the self-assembled structure. The orientations of the NRs are not random, rather some spots are recognized in the pattern, which can be indexed as the  $[110]$  diffraction pattern of a face-centered cubic structure. This pattern indicates that the nanorods are preferentially oriented along  $[110]$  orientation. Alternatively, an electron diffraction pattern recorded from another area shows a  $[100]$  orientation of the NRs (Figure 5b). These results are possible because our previous study indicates that the nanorods have  $\{110\}$  and  $\{100\}$  facets, which are likely to be the contacting faces onto the substrate while the self-assembly is formed.

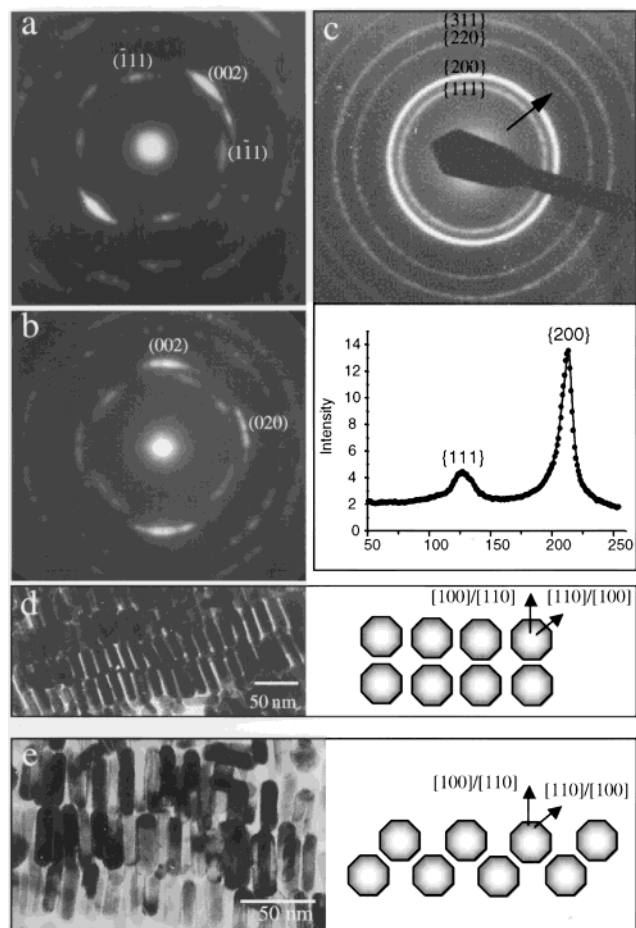


**Figure 5.** (a) Typical selected area electron diffraction (SAD) pattern from an area, with [001] preferred orientation. (b) Electron diffraction pattern recorded from a large area and corresponding intensity profile across the {111} and {200} rings. (c) Selected area diffraction (SAD), from a region with [110] preferred orientation. Two different packing regimes of NRs and their corresponding model. (d) Face to face stacking of NRs. This assembly consists of at least 3 layers of particles; because of their face to face packing, it seems like a monolayer of particles. (e) Second type of packing showing stacking of NRs with a lateral displacement. The overlap of NRs is clearly shown in the image.

If we enlarge the size of the selected area aperture to include an area of 20  $\mu\text{m}$  in diameter, a ring pattern is observed (Figure 5c). It is important to note that the {200} ring is stronger than {111} ring, as shown by the intensity profile given below the diffraction pattern. A line scan across the first two rings gives an intensity profile as given in the bottom of Figure 5c. From kinematic electron diffraction theory, the {111} reflection is not observed if the crystal is oriented in the [100] direction. Since the scattering factor for the {111} reflection is about 10% larger than that of the {200} reflection, the intensity of the {111} ring would be 20% stronger than that of the {200} ring if the NRs were oriented randomly. In contrast, a much stronger intensity of the {200} ring in Figure 5c shows that [100] is the preferred orientation of the NRs. A quantitative analysis of the diffraction intensity can provide the relative percentage of the gold nanorods oriented along [100] and other orientations.

From kinematic electron diffraction theory, the intensity ratio of the {111} and {200} reflection rings is directly related to the number of nanorods oriented along [001] and those oriented randomly by

$$\frac{I_{\{200\}}}{I_{\{111\}}} = \frac{f_{\{200\}}^2 n_{\{001\}}}{f_{\{111\}}^2 n_{\text{random}}}$$

where  $I_{\{200\}}$  and  $I_{\{111\}}$  are the experimentally measured intensities of the {200} and {111} rings from Figure 5c, respectively, and  $f_{\{200\}}$  and  $f_{\{111\}}$  are the electron scattering factor of a gold atom for the scattering angles corresponding to {200} and {111} rings, respectively. The ratio of  $f_{\{200\}}/f_{\{111\}}$  is 0.917, for 200 kV electrons.<sup>21</sup> An analysis for a total of 10 groups of data, collected from the diffraction rings in Figure 5b, gives  $n_{\{001\}}/n_{\text{random}} = 0.90 \pm 0.07$ , indicating a highly [001] orientated ordering in the self-assembly.

The ring pattern given in Figure 5c indicates that the entire self-assembly is composed of local ordered domains. Each domain has a superlattice structure, while there is no in-plane orientational correlation among the domains. This is similar to the texturing of crystal grains in thin film growth, where single crystal domains grow independently of each other and join together to produce a thin film.

TEM images also reveal the stacking sequence of the nanorods (Figure 5d,e), from which the following two stacking models are proposed, considering the {110} and {100} faceted shape of the gold nanorod cross-section. In the first model (Figure 5d), the nanorods are oriented in [100], and the second layer can stack on top of the first layer without lateral translation; thus, the {100} faces are directly facing {100} faces of the other NR in the second layer. In the second model (Figure 5e), the second layer can stack onto the first layer, but with a lateral displacement so that the nanorods in the second layer are located halfway between the nanorods in the first layer. This is the case of {110} directly facing {110}. In the [110] texturing case, the two models presented above are the same except exchanging the location of the {110} and {100} facets. In the models presented here, a common characteristic of the self-assembly of the nanoparticles is face-to-face, which was proven to be the most stable configuration for self-assembly.<sup>22,23</sup>

## Discussion

**Mechanism of Formation of Nanorod Arrays.** An interesting observation that needs to be discussed is the formation of arrays of nanorods at the contact line of the solution and the substrate. A similar pattern is observed on the substrate in all of the deposited samples. As we move below the initial contact line of the nanoparticle solution and substrate, the thickness of the assembly shows a slow increase, reaches a maximum, and then abruptly decreases. This behavior is shown qualitatively in Figure 1. Dimitrov et al.<sup>24</sup> observed the same behavior while producing monolayers of spherical polystyrene particles. In their approach, a clean wettable glass substrate was dipped into a suspension of polystyrene particles. When the substrate was kept stationary, they found that monolayers and successive multilayers of particle arrays spontaneously start to form on the substrate from the substrate–solution–air contact line down to the bulk solution. The similarity of our results with those of Dimitrov et al.<sup>24,25</sup> suggests that a similar model can be applicable to explain the self-assembly of gold nanorods.

According to this model, the lateral immersion or capillary forces may be one of the main factors causing the observed self-assembly of small colloidal particles confined in thin films. This force depends on the interparticle separation, particle radius, and surface tension of the liquid, and therefore the meniscus deformation around particles. Two main steps are involved in the self-assembly process: (1) convective transfer of particles

from the bulk of the solution to the thin film due to water evaporation from the thin film;<sup>26</sup> (2) interactions between the particles in the thin film that lead to specific structures. The primary driving force for the convective transfer of particles is the water evaporation from the film surface. When the water evaporates, the curvature of the menisci between the particles increases, which consequently increases the capillary pressure or capillary interparticle forces. Also, due to the thinning of the film, the disjoining pressure of the film increases.<sup>27</sup> Therefore, as water evaporates, the pressure of the thin film on the substrate compared to the pressure in the suspension decreases. This pressure gradient ( $\Delta P$ ) produces a suspension influx from the bulk solution toward the thin film. The influx consists of water and nanoparticle flux components. The water flux compensates for the evaporated water from the film, and the nanoparticle flux causes particle accumulation in the film. After carrying the particles from the bulk solution toward the array's leading edge, the water influx presses the particles to the array, thus forming dense assemblies. According to this model, because of the hydrostatic pressure, the thickness of the vertical film increases from the substrate–air–solution contact line downward toward the solution. Successive monolayers and bilayers are expected to be formed as the continuous particle flux fills up the space between the substrate and the film surface. Experimental results from Dimitrov et al.<sup>24</sup> show formation of multilayers when a wettable plate dipped in a suspension of fine particles was kept stationary. This is consistent with the formation of monolayers as well as the multilayers of the nanorods as one moves away from the three-phase interface toward the solution.

In explaining the tendency of nanorods to align parallel to each other, one reason could be the higher lateral capillary forces along the length of a nanorod as compared to its width. For spherical particles, it is shown that the lateral capillary force is proportional to  $R^2$ , in which  $R$  is the diameter of the particle.<sup>27</sup> This anisotropy of interaction between nanorods could be one important driving force for the side by side alignment of nanorods rather than end to end. In addition to this force, in the experiment performed by the Nagayama group,<sup>25</sup> the packing of the particles in the thin film is also considered to be dependent on the hydrodynamic pressure of the water stream. These forces are dependent on the pressure gradient ( $\Delta P$ ), which is a function of the thickness of the wetting film. But a decrease in the thickness of the film leads to an increase in the friction force between the substrate and particles, which may lead to the formation of smaller domains. The above model seems to explain our observed results. The small nanoparticle assemblies observed in some of our experiments (for example Figure 4) could be a result of fast water evaporation, as explained in Dimitrov et al.'s results. A second source of small assemblies and lack of alignment could be due to the fact that the contact line between small size substrates (TEM grids) and the solution are not ideal for these types of experiments, because the length of the horizontal part of the contact line is short.

TEM observations also revealed that after the formation of mono- and multilayers of the nanorods, the amount of deposited sample abruptly decreases and only scattered particles are observed on the substrate. This could be attributed to the lack of the nanoparticle supply of the solution and therefore a decrease in the nanoparticle influx toward the thin film. Overall, this model seems to explain most of the observed results. Depending on the balance between hydrodynamic and lateral capillary forces, smaller or larger ordered domains could be formed on the substrate.

**Interparticle Forces among NRs.** Interparticle forces can be classified into two main categories: repulsive and attractive. More specifically, for charged colloidal particles, the most commonly used effective pair potential consists of a van der Waals (VdW) attraction and a screened Coulomb repulsion term.<sup>28</sup> Before considering these forces, it is necessary to take into account some characteristics about nanorod structure and its environment. A nanorod includes a metallic core surrounded by a mixture of two surfactants. The headgroup of the surfactant is a quaternary amine, which has a positive charge on nitrogen and a solvated bromide as counterion, which can be in close proximity to the positive charge on the nitrogen or far from the surface of nanoparticle. Therefore, a cylindrical nanoparticle with a length of 54 nm and a width of 12 nm could have a large number of positive charges on its surface.

The concentration of electrolyte can be considered equal to the salt concentration, i.e., 0.05 M (neglecting the free surfactant concentration). In this case, the Debye length is estimated to be  $\sim 1.36$  nm at 25 °C.<sup>29</sup> This length is approximately the thickness of the ionic atmosphere surrounding a NR. The spacing (edge to edge) between two nanoparticles is found to be  $\sim 2.8$  nm, which is larger than the Debye length. This suggests, the absence of a strong repulsive force between two particles at this interparticle spacing, as compared to the case where the spacing is less than 1.36 nm.

In the macroscopic scale, the above fundamental forces are exhibited in a more visible form. Here the forces, which were mentioned in the Discussion, are briefly discussed. When a particle protrudes from an aqueous layer, with a wettable surface, lateral capillary forces appear because of the meniscus deformation. In fact, the lateral capillary force is a result of the perturbation of the shape of the liquid meniscus around a given particle caused by the presence of the second particle. The larger the interfacial deformation created by the particles, the stronger the capillary interaction between them. The lateral capillary forces have two components.<sup>27</sup> One is the integral of surface tension along the contact line of solution and a given nanoparticle. The second is the integral of hydrostatic pressure throughout the particle surface. The disjoining pressure,  $\Pi$ , defines the force of interaction of two planes separated by a thin film. A positive value of  $\Pi$  corresponds to repulsion, and a negative value, to attraction. Also, this force contains several components of electrostatic repulsion, van der Waals, solvation, and steric surface forces.<sup>30</sup>

As mentioned, packing of nanoparticles on the substrate could be a result of the hydrodynamic pressure of water stream and lateral capillary forces. One possible model to rationalize the stability of these positively charged nanoparticles in a closed packed form is the presence of counterions between nanoparticles.<sup>29,31</sup> According to this model, a layer of counterions between two surfaces with the same charges can produce a stable structure. A detailed quantitative theoretical calculation is needed to explain the observed anisotropy in the observed self-assemblies and the interrod distances observed experimentally.

## Conclusion

This work has shown that it is possible to generate self-assemblies of gold nanorods. Varying the experimental conditions can change the dimensionality of the assemblies. Factors such as the rate of water evaporation, the ionic strength, the surfactant concentration, and the particle size and shape distributions are important in this process. Additionally, it was shown how the method of deposition can improve the quality of the assembly. This method produces a thin film of solution

on the substrate, which is supplied by the bulk solution. Evaporation of water from the thin film can increase the lateral capillary forces between particles and also build up a pressure gradient, which leads to the packing of nanoparticles at the contact line of the solution and the substrate.

**Acknowledgment.** This research was supported by NSF CHE-9727633. B.N. would like to thank Molecular Design Institute (MDI) at Georgia Tech for partial financial support. We also thank the Georgia Tech Electron Microscopy Center for providing the research facilities.

## References and Notes

- (1) (a) Brus, L. E. *J. Chem. Phys.* **1983**, *79*, 5566. (b) Stucky, G. D.; MacDougall, J. E. *Science* **1990**, *247*, 669. (c) Roychowdhury, V. P.; Janes, D. B.; Bandyopadhyay, S.; Wang, X. *IEEE, Trans. Electron Devices* **1996**, *43*, 1688. (d) Alivisatos, A. P. *Science* **1996**, *271*, 933. (e) Schmid, G. *Chem. Rev.* **1992**, *92*, 1709.
- (2) (a) Tohno, S.; Itoh, M. *J. Aerosol Sci.* **1993**, *24*, 339. (b) Whetten, R. L.; Khoury, J. T.; Alvarez, M. M.; Murthy, S.; Vezmar, I.; Wang, Z. L.; Stephens, P. W.; Cleveland, C. L.; Luedtke, W. D.; Landman, U. *Adv. Mater.* **1996**, *8*, 428. (c) Herron, N.; Calbrese, J. C.; Farneth, W. E.; Wang, Y. *Science* **1993**, *259*, 1426. (d) Vossmeier, T.; Katsikas, L.; Giersig, M.; Popvic, I. G.; Diesner, K.; Chemsiddine, A.; Eychmuller, A.; Weller, H. *J. Phys. Chem.* **1994**, *98*, 4109. (e) Feldheim, D. L.; Gragbar, K. C.; Natan, M. J.; Mallouk, T. E. *J. Am. Chem. Soc.* **1996**, *118*, 7640.
- (3) (a) Korgel, B. A.; Monbouquette, H. G. *J. Phys. Chem.* **1996**, *100*, 346. (b) Steigerwald, M. L.; Alivisatos, A. P.; Gibson, J. M.; Harris, T. D.; Kortan, R.; Muller, A. J.; Thayer, A. M.; Duncan, T. M.; Douglass, D. C.; Brus, L. E. *J. Am. Chem. Soc.* **1988**, *110*, 3046. (c) Colvin, V. L.; Schlamp, M. C.; Alivisatos, A. P. *Nature* **1994**, *370*, 354. (d) Collier, C. P.; Saykally, R. J.; Shiang, J. J.; Henrichs, S. E.; Heath, J. R. *Science* **1998**, *277*, 1978. (e) Schmid, G., Ed. *Clusters and Colloids: From theory to application*; VCH: Weinheim, 1994. (f) Schmid, G., Ed. *Clusters and Colloids: From theory to application*; VCH: Weinheim, 1994.
- (4) (a) Brust, M.; Walker, M.; Bethell, D.; Schiffrin, D. J.; Whman, R. J. *Chem. Soc., Chem. Commun.* **1994**, 802. (b) Leff, D. V.; Ohara, P. C.; Heath, J. R.; Gelbart, W. M. *J. Phys. Chem.* **1995**, *99*, 7036. (c) Tanori, J.; Pileni, M. P. *Langmuir* **1997**, *13*, 639–646. (d) Pileni, M. P.; Motte, L.; Billoudet, F.; Mahrt, J. Willig, F. *Mater. Lett.* **1997**, *31*, 255. (e) Herron, N.; Wang, Y.; Eddy, M. M.; Stucky, G. D.; Cox, D. E.; Moller, K.; Bein, T. *J. Am. Chem. Soc.* **1989**, *111*, 530. (f) Kane, R. S.; Cohen, R. E.; Silbey, R. *Chem. Mater.* **1996**, *8*, 1919.
- (5) See for example: Ohara, P. C.; Leff, D. V.; Heath, J. R.; Gelbart, W. M. *Phys. Rev. Lett.* **1995**, *75*, 3466.
- (6) Wang, Z. L.; Harfenist, S. A.; Whetten, R. L.; Bentley, J.; Evans, N. D. *J. Phys. Chem.* **1998**, *102*, 3068.
- (7) Harfenist, S. A.; Wang, Z. L.; Alvarez, M. M.; Vezmar, I.; Whetten, R. L. *J. Phys. Chem.* **1996**, *100*, 13904.
- (8) Murray, C. B.; Kagan, C. R.; Bawendi, M. G. *Science* **1995**, *270*, 1335.
- (9) Motte, L.; Billoudet, F.; Lacaze, E.; Douin, J.; Pileni, M. P. *J. Phys. Chem. B* **1997**, *101*, 138.
- (10) Whetten, R. L.; Shafiqullin, M. N.; Khoury, J. T.; Schaaff, T. G.; Vezmar, I.; Alvarez, M.; Wilkinson, A. *Acc. Chem. Res.* **1999**, *32*, 397.
- (11) Magruder, R. H.; Yang, L.; Haglund, R. F. Jr. *Appl. Phys. Lett.* **1993**, *62*, 1730.
- (12) Heitman, D.; Kothaus, J. P. *Phys. Today* **1993**, 56.
- (13) Kagan, C. R.; Murray, C. B.; Nirmal, M.; Bawendi, M. G. *Phys. Rev. Lett.* **1996**, *76*, 1517.
- (14) Korgel, B. A.; Fitzmaurice, D. *Adv. Mater.* **1998**, *10*, 661.
- (15) Ying, Y.; Chang, S. S.; Lee, C. L.; Wang, C. R. C. *J. Phys. Chem. B* **1997**, *101*, 6661.
- (16) The extinction coefficient for nanorods is not exactly known.
- (17) Wang, Z. L. *Adv. Mater.* **1998**, *10*, 13.
- (18) Wang, Z. L.; Harfenist, S. A.; Vezmar, I.; Whetten, R. L.; Bentley, J.; Evans, N. D. *Adv. Mater.* **1998**, *10*, 808.
- (19) Wang, Z. L. *J. Phys. Chem. B* **2000**, *104*, 1153.
- (20) Wang, Z. L.; Mohamed, M. B.; Link, S.; El-Sayed, M. A. *Surf. Sci.* **1999**, *440*, 809.
- (21) Doyle, P. A.; Turner, P. S. *Acta Crystallogr.* **1968**, *A24*, 390.
- (22) Wang, Z. L. *Characterization Mater.* **1999**, *42*, 101.
- (23) Korgel, B. A.; Fullam, S.; Connolly, S.; Fitzmaurice, D. *J. Phys. Chem. B* **1998**, *102*, 8379.
- (24) Dimitrova, A. S.; Nagayama, K. *Langmuir* **1996**, *12*, 1303.
- (25) Kralchevsky, P. A.; Denkov, N. D.; Paunov, V. N.; Velev, O. D.; Ivanov, I. B.; Yoshimura, H.; Nagayama, K. *J. Phys.: Condens. Matter* **1994**, *6*, A395.
- (26) Denkov, N. D.; Velev, O. D.; Kralchevsky, P. A.; Ivanov, I. B.; Yoshimura, H.; Nagayama, K. *Nature* **1993**, *361*, 26.
- (27) The origin of the disjoining pressure is the capillary interactions between colloidal particles, which are governed by the surface forces. For more reading see: Kralchevsky, P. A.; Nagayama, K. *Langmuir* **1994**, *10*, 23.
- (28) Derjaguin, B. V.; Landau, L. D. *Acta Physicochim.* **1941**, URSS 14, 633. Verwey, E. J. W.; Overbeek, J. T. G. *Theory of the Stability of Lyophobic Colloids*; Elsevier: Amsterdam, 1948.
- (29) Israelachvili, J. N. *Intermolecular and Surface Forces*, 2nd ed.; Academic Press: New York, 1985.
- (30) Derjaguin, B. V.; Rabinovich, Y. I.; Churaev, N. V. *Nature* **1978**, *272*, 313.
- (31) See for example: Tehver, R.; Ancilotto, F.; Toigo, F.; Koplik, J.; Banavar, J. *Phys. Rev. E* **1999**, *59*, 1335.